Comparison of lower stratospheric tropical mean vertical velocities

M. R. Schoeberl,[1] A. R. Douglass,[1] R. S. Stolarski,[1] S. Pawson,[1] S. E. Strahan,[2] and W. Read[3]

[1] We have analyzed 13 years (1993–2005) of tropical stratospheric water vapor data from the Halogen Occultation Experiment and over 3 years of data (October 2004 through November 2007) from the Aura Microwave Limb Sounder. By correlating the phase lag of the water vapor "tape recorder" signal between levels we estimate the time mean vertical velocity. Our estimated vertical velocity compares well with calculations from the Goddard Earth Observing System (GEOS) chemistry-climate model (CCM) and from the GEOS data assimilation system. Between 18 and 26 km both the GEOS CCM simulations and water vapor observations agree that the vertical velocity is below 0.04 cm/s, with a minimum near 20 km of 0.03 cm/s. Vertical velocities deduced from water vapor observations are higher than those from the GEOS CCM in the region 16–18 km (0.04 cm/s) and above 26–30 km (up to 0.07 cm/s). These estimates are close to earlier estimates from a shorter water vapor record and radiative transfer models. No evidence is found for velocities as high as 0.15 cm/s as was recently estimated from aircraft CO_2 measurements in the upper troposphere/lower stratosphere. Further diagnosis of the aircraft CO_2 data and model simulations of CO_2 show that while the CO_2 data give an apparent upward transport velocity of ~0.06 cm/s, about half of this is due to vertical and horizontal eddy transport. Accounting for the eddy terms gives a CO_2-based estimate of the vertical velocity of ~0.03 cm/s, in much closer agreement with that estimated from water vapor.

Citation: Schoeberl, M. R., A. R. Douglass, R. S. Stolarski, S. Pawson, S. E. Strahan, and W. Read (2008), Comparison of lower stratospheric tropical mean vertical velocities, *J. Geophys. Res.*, *113*, D24109, doi:10.1029/2008JD010221.

1. Introduction

[2] The water vapor concentration in the tropical upper troposphere varies because of seasonal variations in temperature and dehydration processes. These variations in water vapor are carried upward by the Brewer-Dobson circulation (BDC) as was first discovered by *Mote et al.* [1996, 1998] using Upper Atmosphere Research Satellite (UARS) observations. In popular terms, the upward propagation of water vapor variations is called the "tape recorder." Observations show that the tape recorder extends from below the tropical tropopause (~16 km) to ~30 km. The existence of the tape recorder tells us that the tropics are very isolated from midlatitude eddy activity in this altitude range. Yet the tape recorder is still linked to midlatitude eddies through the strength of the BDC that is controlled by the dissipation of extratropical planetary waves in the midstratosphere [*Haynes et al.*, 1991]. Thus, the upwelling strength varies seasonally because of the relative higher eddy activity in the Northern Hemisphere, as well as interseasonally because of other effects, for example the

North Atlantic Oscillation [*Randel et al.*, 2006]. More detail on the linkage between the BDC and tropical and midlatitude eddy activity can be found in the work of *Kerr-Munslow and Norton* [2006], *Norton* [2006], *Shepherd* [2007], and *Randel et al.* [2008].

[3] Any trace gas that has a temporal variation in its mixing ratio near the tropical tropopause and has a lifetime greater than a few months in the lower stratosphere can produce a tape recorder signal. For example, CO varies seasonally at the tropical tropopause because of annual variations in the Brewer-Dobson circulation and thus produces a tape recorder signal [*Schoeberl et al.*, 2006, 2008]. A tape recorder is also evident in HCN, which is occasionally enhanced by biomass burning [*Pumphrey et al.*, 2008], and in CO_2 which has an annual cycle because of biospheric variations [*Andrews et al.*, 1999, *Park et al.*, 2007].

[4] *Mote et al.* [1996] estimated a vertical velocity between 16 and 32 km of 0.02–0.04 cm/s from the tape recorder signal. *Mote et al.* [1998] then used the dissipation of the H_2O tape recorder signal with altitude to diagnose the degree of midlatitude mixing. Consistent with earlier studies of the quasi-biennial oscillation (QBO) [e.g., *Dunkerton* 1991; *Schoeberl et al.*, 1997], they found that the horizontal eddy mixing rate was very small in the tropical lower stratosphere. At 22 km the mixing time scale was ~80 months. Above 26 km, however, the mixing time scale was estimated to be less than 20 months. The low levels of tropical-midlatitude mixing imply that the most important

---
[1]NASA Goddard Space Flight Center, Greenbelt, Maryland, USA.
[2]Goddard Earth Science and Technology Center, University of Maryland, Baltimore County, Baltimore, Maryland, USA.
[3]Jet Propulsion Laboratory, California Institute of Technology, Pasadena, California, USA.

dynamical processes in the tropical lower stratosphere are the mean upwelling by the BDC and circulation changes due to the QBO [*Baldwin et al.*, 2001; *Niwano et al.*, 2003; *Schoeberl et al.*, 2008]. In this paper, we use the water vapor tape recorder to estimate the stratospheric mean vertical velocity in the tropics, as was done by *Mote et al.* [1996], and compare it to model estimates of that quantity. *Mote et al.* [1996] simply observed the distance the maximum in the water vapor signal traveled over the measurement period and estimated the vertical velocity. *Niwano et al.* [2003] also estimated the vertical velocity from the Halogen Occultation Experiment (HALOE) water vapor and methane data for the period November 1991 to December 1999 by correlating the tracer phase lag between measurement levels. Their work focused on the estimating the vertical velocity perturbation associated with the mid-stratospheric QBO. In this paper we will analyze the vertical velocities in the tropical lower stratosphere. More recently, *Corti et al.* [2006] have emphasized the role of cirrus cloud radiative heating along with deep convection in boosting air from the level near 350 K (13–14 km), where most cloud detrainment occurs, to the region where net clear-sky radiative processes switch from cooling to heating at about 360 K. In other words, the heating by cirrus pushes the zero net heating level down to about 14 km. The inclusion of cirrus heating increases the radiative driven vertical velocity in the 14–16 km region. Our approach in diagnosing the vertical velocity is similar to that of *Niwano et al.* [2003], but we examine the correlation over a longer HALOE period and we include the recent Aura data.

2. Description and Validation of the Analysis Technique

[5] In this section, the technique is introduced for estimating the vertical velocity from the tropical water vapor distribution. The method is tested using output from the Goddard Earth Observing System (GEOS) chemistry-climate model (CCM).

2.1. H$_2$O Simulated in the GEOS CCM

[6] *Pawson et al.* [2008] describe version 1 of the GEOS CCM. Version 1 combines version 4 of the GEOS general circulation model (GEOS-4 GCM [*Bloom et al.*, 2005]) with the stratospheric chemistry module from the Goddard Chemistry–Transport Model [*Douglass et al.*, 2003]. A GEOS CCM simulation of past climate [*Pawson et al.*, 2008] is used here. The run was constrained by observed concentrations of greenhouse gases and halogens imposed at the lowest model layer and by observed sea surface temperature (SST) and sea ice concentrations from Hadley Center analyses (HadISST) [*Rayner et al.*, 2003]. A comparison of numerous CCM simulations of the atmosphere in the late 20th Century [*Eyring et al.*, 2006] revealed that this GEOS CCM run accurately simulates many aspects of the atmospheric structure. In particular, realistic simulation of the tropical tropopause temperatures and their seasonality [*Pawson et al.*, 2008] produce a realistic "tape recorder" signal (see Figure 1a) that propagates at a rate consistent with observed values [*Oman et al.*, 2008]. *Eyring et al.* [2006] show that many CCMs do not represent the ampli-

tude, phase and propagation speed of the tape recorder signal as accurately as the GEOS CCM.

2.2. Method for Analyzing the Vertical Velocity

[7] The phase-lagged correlation coefficient between adjacent levels is used to estimate the vertical velocity as in the work of *Niwano et al.* [2003]. The water vapor data are interpolated onto a daily grid (if needed), and the data at the upper level are shifted in 1-day increments up to 14 months. The peak in the correlation between the data at the lower level and the phase-shifted data at the upper level is assumed to be the trace of the signal propagating between levels. The vertical velocity is then simply the distance between the levels divided by the signal propagation time between the levels, which is the time lag at which the correlation peaks. The vertical velocity is assigned to the midpoint between the levels. More explicitly, zonal mean tracer transport is governed by $\frac{\partial \bar{\mu}}{\partial t} + w^* \frac{\partial \bar{\mu}}{\partial z} + v^* \frac{\partial \bar{\mu}}{\partial y} = \frac{\partial}{\partial z} K_{zz} \frac{\partial \bar{\mu}}{\partial z} + \frac{\partial}{\partial y} K_{yy} \frac{\partial \bar{\mu}}{\partial y}$ (see *Andrews et al.* [1987, equation 9.4.13] for notation). The star indicates the residual vertical velocities, K is the turbulent mixing coefficients (eddy mixing is included in the residual circulation terms), and μ is the trace gas mixing ratio. The overbar indicates zonal mean. For the tape recorder, the turbulent mixing fluxes are usually neglected and in the tropics, meridional advection is weak so $\frac{\partial \bar{\mu}}{\partial t} + w^* \frac{\partial \bar{\mu}}{\partial z} = \frac{d \bar{\mu}}{dt} = 0$. Tracking the vertical propagation of the tracer gradient is effectively a Lagrangian calculation. If the assumption that the mixing terms can be neglected is incorrect then the estimate of the vertical velocity will be uncertain. Consider the case of strong turbulent mixing which reduces the vertical gradient. The vertical mixing will couple the different levels and reduce the time lag giving a larger estimate for the vertical velocity. This means that vertical velocities computed by correlating the lag between levels will likely be an upper bound on the actual vertical velocity.

[8] In practice, when the correlation between two levels has a lag of less than one month it usually means the either the signal is too weak to provide a good estimate of propagation speed or there are anomalous values in the water vapor data. If there are two peaks in the lag correlation within 18 months then the shortest lag period is chosen. Our procedure may overestimate the signal propagation speed in those rare two-peak cases. Data from 16 km to 32 km are processed from all data sets used in this study but the data above 28 km is quite noisy and is not shown. At each level, we identify vertical velocities that are two standard deviations (σ) from the mean as "problematic" estimates. The problematic estimates are removed from the final data set.

[9] The overall uncertainty in the calculation includes instrumental measurement error and sampling error (that is, using only a few HALOE profiles to represent the tropical monthly mean). It is nearly impossible to do a strict error budget analysis on the combined data sets. Instead, we will use the standard deviation of the vertical velocity fields at each level as a measure the uncertainty in the calculation.

2.3. Validation of the Method Using GEOS CCM Data

[10] Figure 1 shows 30-year time series between 16 and 28 km of the monthly mean water vapor concentrations from the GEOS CCM and the estimated vertical velocities
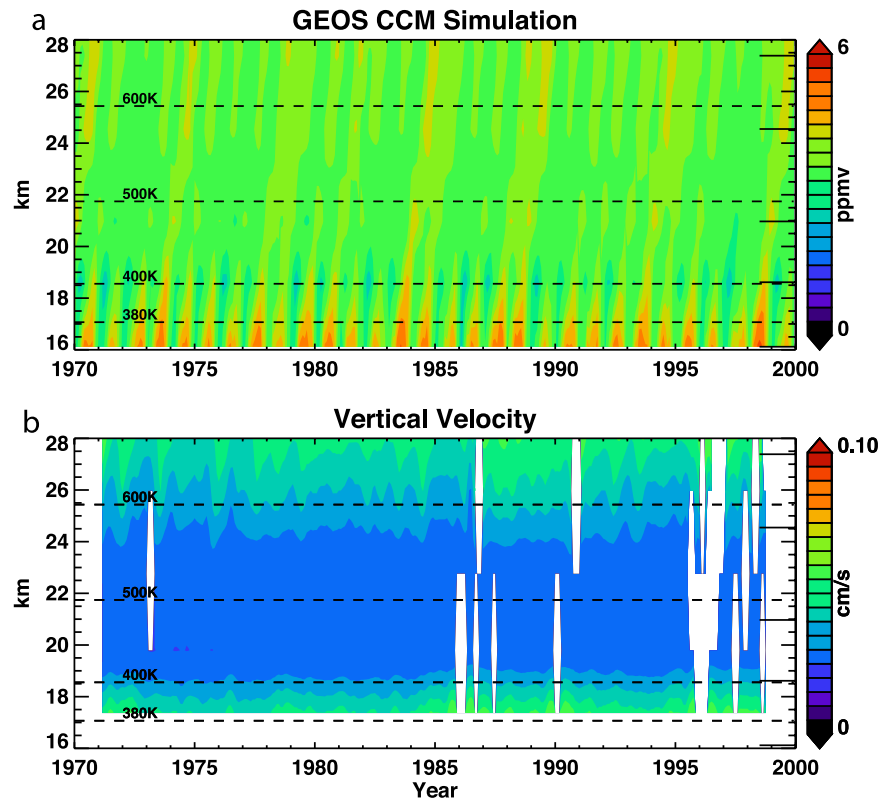
a **GEOS CCM Simulation**

b **Vertical Velocity**

Figure 1. (a) The GEOS CCM zonal mean equatorial water vapor concentration versus time. (b) The zonal mean vertical velocity estimated from correlating the water vapor between levels. Dashed lines show the approximate latitude of the potential temperature levels indicated. White regions indicate areas where the vertical velocity could not be estimated. Long tick lines on the right show the model levels.
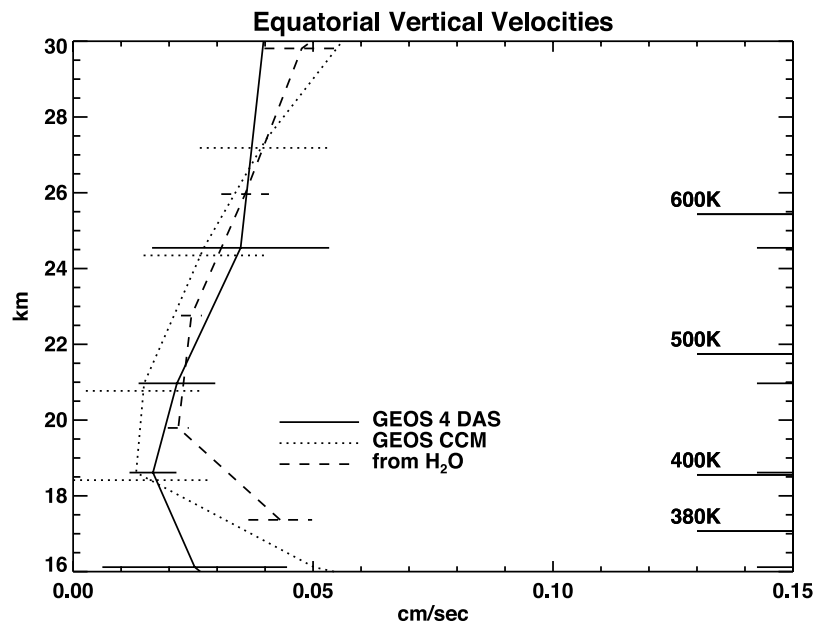
Equatorial Vertical Velocities

GEOS 4 DAS
GEOS CCM
from H₂O

Figure 2. Comparison between time mean GCM vertical velocities and vertical velocities derived from the upward propagation of water vapor anomalies. Horizontal lines represent one standard deviation from the time mean vertical velocity. GEOS CCM uses the GEOS-4 GCM. "From H_2O" is the vertical velocity diagnosed from the GEOS CCM using the water vapor tape recorder simulation. Right-hand tick marks show the potential temperature levels. Long unlabeled tick lines on the right show the model levels.
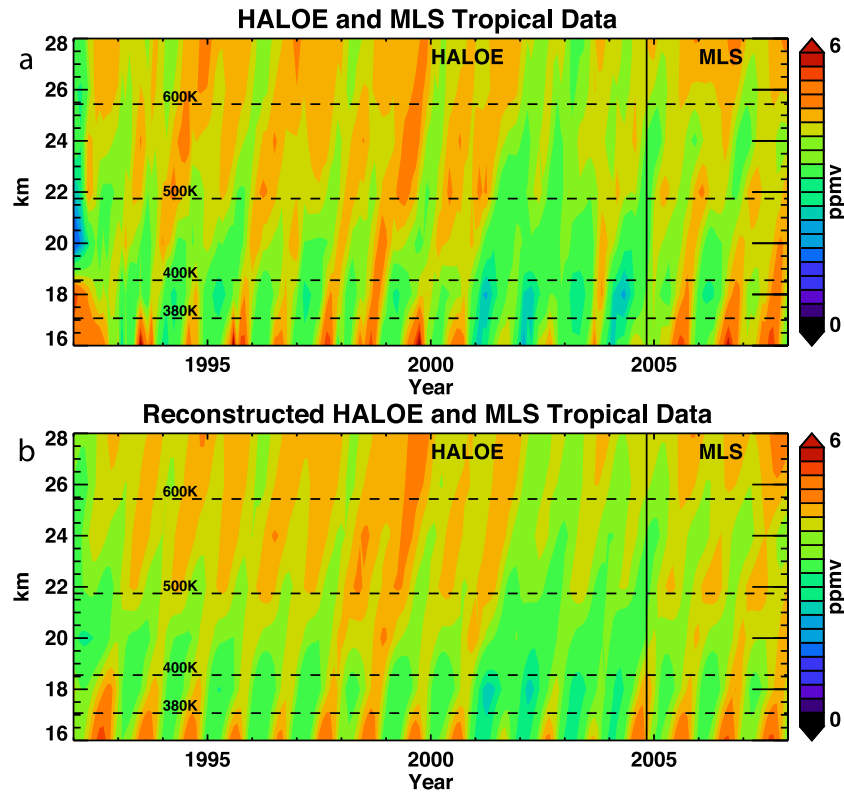
Figure 3. (a) Combined Halogen Occultation Experiment (HALOE) and Microwave Limb Sounder (MLS) water vapor time series at the equator. (b) Reconstructed data set using multiple parameter fit of the data to reduce the noise as described in text. Approximate potential temperature levels are shown as dashed lines. Long tick lines on the right show the model levels.

at the equator computed using the lag correlation method. The H_2O tape recorder signal is clearly evident in Figure 1a.

[11] Figure 1b shows the vertical transport velocity derived using the correlation method. This should be approximately the monthly mean residual vertical velocity (assuming that the tropical eddies are linear, steady, and adiabatic [Andrews et al., 1987, equation 9.4.13]). As expected, the correlation method works best for periods where there is either a positive or negative anomaly strongly connecting adjacent levels. There also periods where the signal appears to vanish or cases where 2 years appear to merge. At these points, the interlevel correlation shows little phase lag and a high vertical velocity is computed and rejected. The vertical velocity shows a minimum at 20 km, increasing slowly above that altitude. Weak annual variations at 20 km are also evident with higher values in winter and lower values in summer. These are the annual variations in the Brewer-Dobson circulation.

[12] Figure 2 shows the time mean vertical velocity from the GEOS CCM compared with the tape recorder estimate. Overall the agreement is quite good and within the uncertainty of the calculations. The only exception is in the upper tropopause region (below 18 km) where the vertical velocity estimate from H_2O is larger than the models. In this region vertical mixing may be reducing the tilt of the tape recorder signal with altitude. This would be interpreted by our method as a higher vertical velocity since we assign all the signal propagation to the mean vertical velocity. This

point will be discussed further below when we analyze the CO_2 data from the model.

[13] A further check on the reality of the GEOS CCM vertical velocities is attained by comparison with values derived from the meteorological fields in the GEOS-4 data assimilation system (DAS) [Bloom et al., 2005]. The time average vertical velocity for 2005–2006 (the early part of the Aura Microwave Limb Sounder (MLS) period) is also shown in Figure 2. The GEOS-4 DAS vertical velocities are in reasonably good agreement, but that from the DAS is about 20–25% larger than the GEOS CCM in the 19- to 26-km layer. This is the region where Pawson et al. [2008] showed that the tape recorder signal propagates upward too rapidly in the GEOS-4 DAS. The DAS vertical velocities are 6 h time averages which significantly improves the fidelity of the vertical transport. The vertical velocities shown in Figure 3 are also in good agreement with ECMWF ERA 40 and NCEP reanalysis vertical velocities shown by Randel et al. [2008, Figure 3].

3. Vertical Velocities Derived From Observations

3.1. Observational H_2O Data

[14] As noted above, the tape recorder was first discovered in satellite water vapor data from the UARS HALOE and MLS observations. HALOE made a nearly continuous record of tropical water vapor data from 1991 to late 2005. We avoid the pre-1992 HALOE data because of retrieval problems associated with the dense Pinatubo stratospheric

Table 1. Data Sets Used in This Study

Data Set	Data Length	Frequency
HALOE-MLS	1992 to Apr 2008	monthly zonal mean
Reconstructed HALOE-MLS	1992 to Apr 2008	monthly zonal mean
Aura MLS	Oct 2004 to Apr 2008	daily zonal mean
GEOS CCM (uses GEOS-4 GCM)	30 years (1970–2000)	monthly zonal mean
GEOS-4 DAS	1992–2007	daily
GMI (uses GEOS-4 GCM)	15 years	daily

aerosols. The HALOE data has over a year overlap with Aura MLS data. The latter ranges August 2004 to the present, although we begin our use of Aura MLS data in October 2004 after which the data is more or less continuous, to March 2008. The two data sets together provide slightly more than 16 years of stratospheric water vapor data record (Table 1).

[15] To begin the analysis, zonal monthly mean v19 HALOE [*Russell et al.* 1993] and V2.2 monthly and daily zonal mean Aura MLS water vapor [*Waters et al.*, 2006, *Read et al.* 2007] data sets were constructed. In the case of HALOE, the data were binned into 5° latitude zones. For MLS, the data were binned into 2° latitude zones. Where occasional missing data occurs in the monthly mean time series, temporal linear interpolation from earlier and subsequent data are used to fill the gap. The monthly mean, zonal mean MLS data is interpolated from the ~3.2 km MLS grid to the ~2 km HALOE vertical grid and the two data sets are combined to produce a long time series. Although there is a jump in the data between HALOE and MLS (as reported by *Lambert et al.* [2007]) this will have no effect on our correlation method since the tape recorder perturbation moves seamlessly across the two data sets.

[16] Figure 3a shows the combined HALOE and MLS data sets at the equator. Although the water vapor tape recorder is clearly visible in the combined data, the HALOE portion of the data set shows less vertical coherence than the MLS data set. Some of this lack of coherence is due to missing data that has been filled in through interpolation. Below we will also use the daily zonal mean MLS data to test the effect of higher time fidelity in the estimates of the

level correlation coefficients. The daily MLS data is on the MLS L2 vertical grid (about 3 km) described in their user's manual [*Waters et al.*, 2006].

[17] Because the HALOE-MLS set is relatively noisy because of the gaps in the HALOE data we have generated a "reconstructed" data set by performing a singular value decomposition based fit to the data assuming linear trends as well as annual, QBO and long-term oscillations as described by *Schoeberl et al.* [2008] (Table 1). The data set is then reconstructed from the fit coefficients. This procedure reduces variance due to interpolation while retaining the essential signal. The reconstructed data are shown in Figure 3b. The reconstructed data capture most of the essential tape recorder variability including the relatively dry period from 2001 onward first identified by *Randel et al.* [2006].

3.2. Vertical Velocity Derived From MLS and HALOE Data

[18] Figure 4 shows the vertical velocity estimated from the combined MLS and HALOE monthly mean data (Figure 3a). Compared to the GEOS CCM (Figure 1b), the vertical velocity is much more variable. Nonetheless, there is a minimum in the vertical velocity near 20 km consistent with that estimated from GEOS CCM. Figure 5 shows the results using the reconstructed data (Figure 3b). The fit procedure has reduced the noisy behavior below 600 K seen in Figure 4. The minimum just above 20 km is again apparent.

3.3. Vertical Velocity From Daily MLS Fields

[19] The HALOE-MLS data set uses monthly mean vertical velocities. Higher time resolution can be obtained by using the daily MLS water vapor fields. The daily zonal mean equatorial MLS water vapor data and the vertical velocities are shown in Figure 6. The vertical velocities from the MLS daily fields are not filtered for 2σ anomalies. Overall the vertical velocity estimates are similar to those seen with the monthly mean calculations.

[20] Figure 7 shows the vertical velocities and 2σ values, the combined HALOE-MLS data, the HALOE-MLS reconstructed data set, and the MLS daily data. The three water vapor derived vertical velocities show good agreement over the domain $17-27$ km. Above 27 km Figures 4 and 5 show that the method produces inconsistent results as the water
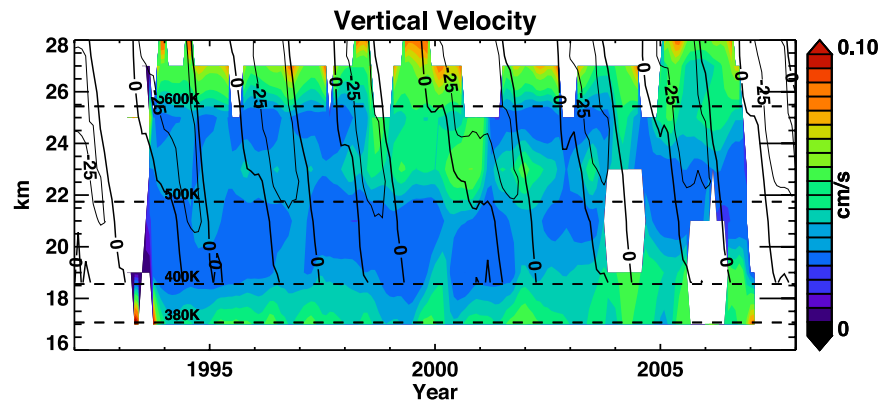

Figure 4. Vertical velocities from merged HALOE-MLS data (Figure 3a). Quasi-biennial oscillation (QBO) winds are represented by solid lines.

Figure 5. Same as Figure 4 except for vertical velocities from reconstructed HALOE-MLS data (Figure 3b).

vapor signal becomes less coherent. The reconstructed data, as might be expected, has lower σ values than the combined data. From 20 to 26 km, the GEOS-4 DAS vertical velocities are also in agreement; below 20 km the GEOS-4 DAS residual vertical velocities are almost a factor of 2 lower than the water vapor derived vertical velocities. The GEOS-4 GCM vertical velocities are also shown. These velocities are also lower than the water vapor derived velocities. The DAS and GCM residual vertical velocities are derived from equation 3.5.1b of *Andrews et al.* [1987] (the Eulerian vertical velocity plus the meridional gradient of the hori-

zontal eddy heat flux). As we show below vertical eddy transport is also important in this region and such transport would carry the water vapor signal up faster than advection by the mean residual vertical velocity. In other words, the DAS dynamics would provide consistent vertical transport but not through the residual vertical velocity.

[21] The values of the vertical velocity are obtained in agreement with the earlier analysis of *Mote et al.* [1996, 1998] using a little over 4 years of UARS MLS and HALOE data, *Niwano et al.* [2003] using 8 years of

Figure 6. (a, b) As in Figure 1 except for MLS data. Version numbers of the MLS data are shown in Figure 6a. Solid lines show the QBO wind velocities (positive eastward). Long tick lines on the right show the model levels.
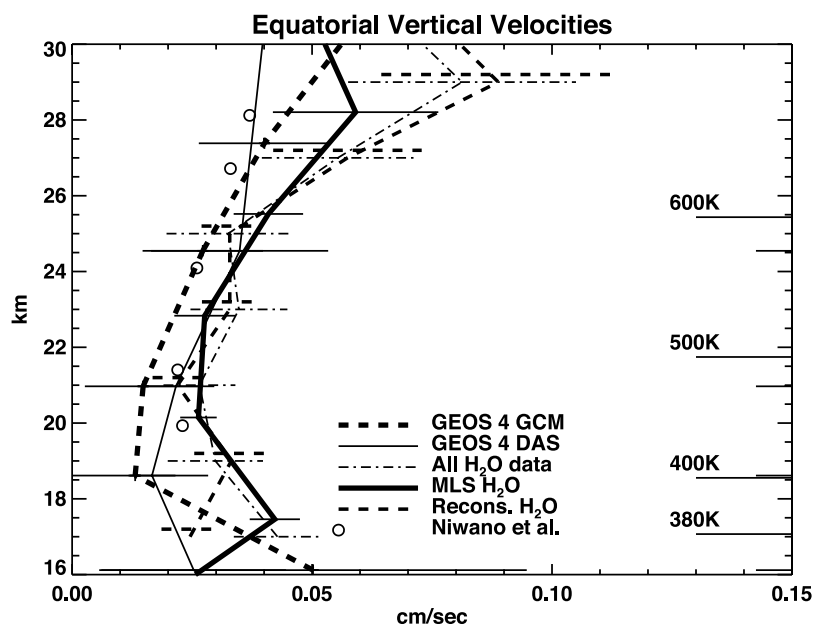
Figure 7. Vertical profiles of time mean vertical velocity. Horizontal lines indicate 2 s from the mean. Circles show the estimated vertical velocities from those given by *Niwano et al.* [2003].

HALOE data, and *Rosenlof et al.* [1997] using radiative transfer calculations.

4. Discussion

[22] To summarize, the vertical transport velocity estimated from the water vapor tape recorder is about 0.04 cm/s near 18 km decreasing to 0.03 cm/s at 21 km then rising to 0.06 cm/s near 27 km. Using diabatic heating rates derived from observed temperature and trace gas fields, *Rosenlof* [1995] and *Eluszkiewicz et al.* [1996] derived tropical lower stratospheric ascent velocities of ~0.02–0.04 cm/s. As mentioned above, *Mote et al.* [1996, 1998] and *Niwano et al.* [2003] derived ascent rates from the water vapor tape recorder of roughly the same value. *Fu et al.* [2007] have recently recomputed tropical heating rates including the heating from ISSCP cloud climatology. Between 17 and 24 km, *Fu et al.* [2007] computed ascent rates that never exceed 0.03 cm/s with values as low as 0.01 cm/s at 19 km. The heating rates of *Corti et al.* [2006] would produce a vertical velocity of about 0.02 cm/s at 16 km slowly decreasing with altitude above that point. Thus, in the region between 20 and 26 km, the models and our data estimates are in good agreement. Below 20 km the radiative transfer models and the GEOS CCM give lower values than our estimate.

[23] Another interesting difference between the water vapor derived velocities and the GEOS CCM vertical velocities is the altitude of the minimum. The water vapor data place the altitude of the minimum at ~21 km, while the models tend to put the minimum closer to 19 km.

4.1. Vertical Velocity and Tracer Transport

[24] The water vapor tape recorder vertical velocity is not equivalent to the Eulerian vertical velocity nor is it exactly the residual vertical velocity (see *Andrews et al.* [1987] for conditions under which the residual vertical velocity is the

transport velocity). *Waugh and Hall* [2002], however, show that for an oscillatory signal in a low-diffusion environment, the mean age of the tracer diagnosed from the tracer oscillations approximates the bulk velocity although vertical mixing will cause the tape recorder to decrease in tilt and thus overestimate the velocity as shown in Figure 7. Nonetheless, the velocity diagnosed from the tape recorder is quite closes to residual vertical velocity.

[25] *Park et al.* [2007] recently used aircraft data measurements of the ascending CO_2 anomalies and the annual CO_2 growth rate to estimate the age of the air emerging from the tropical tropopause layer. From their estimate *Park et al.* [2007] compute an upwelling rate of 0.15 ± 0.03 cm/s at 18 km; this is 3–4 times larger than our estimates from water vapor. These ascent rates are also much higher than ascent rates found in the models described above. One possible explanation for this discrepancy between CO_2 and water vapor ascent rates is that convective processes are injecting surface air into the upper tropical tropopause layer as suggested by *Folkins et al.* [2006] while simultaneously dehydrating the lofted air. Convective injection would reduce the age of the air in the upper troposphere as measured by CO_2 by diluting the lower (older) CO_2 values with younger (higher) CO_2 values. The reduction in age could be interpreted as a result of high vertical velocities. In making their argument, *Folkins et al.* [2006] pointed to the anticorrelation between upper tropospheric ozone and CO as evidence of the coupling between the surface and upper troposphere by convection. However, most convection detrains below 350–360 K (16 km) and only 1.3% of the convection penetrates above 14 km with 0.1% reaching 18 km [*Liu and Zipser*, 2005; *Corti et al.*, 2006]. Thus, it seems unlikely that sufficient young air could be lofted to bias the observations. *Park et al.* [2007] also note that the compact structure of the CO_2 measurements argue against strong vertical mixing above 360 K.
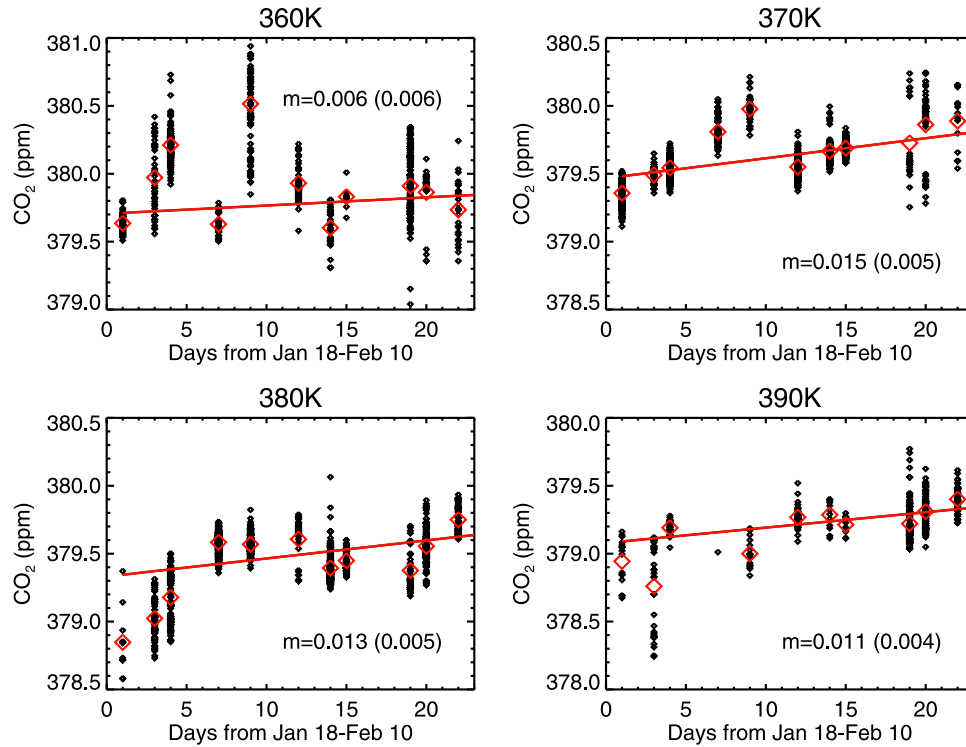
Figure 8. CO_2 measurement from Costa Rica Aura Validation Experiment flights at different isentropic surfaces. Dots show values, red diamond is the mean value of the ensemble, and the red line is a fit to the data; m is the slope of the fitted line (time trend). One standard deviation of the fitted slope is given in parentheses.

4.2. Reanalysis of CO_2 Observations

[26] The difference between the CO_2 analysis of *Park et al.* [2007] and the various model/tape recorder vertical velocities is puzzling. The analysis of *Park et al.* [2007] assumes the Boering proxy [*Boering et al.*, 1996] for stratospheric CO_2 input. In other words, the Mauna Loa + Samoa surface time series can be used at the base of the tropical tropopause layer (TTL), ~360 K potential temperature. In northern winter, this proxy has a slope of 10.8 ppm/a, or 0.0296 ppm/d. *Park et al.* [2007] also assume that the only important transport process in the TTL is vertical advection; horizontal transport and mixing are assumed to be negligible. With these assumptions they propose that the daily observed CO_2 gradients between 360 and 390 K in the tropics can be explained by the simple vertical propagation of a time-varying CO_2 signal at 360 K. That is, the modal age is equal to the mean age.

[27] Their first assumption, that the time trend of CO_2 at 360 K is equal to the winter slope of the Boering proxy, can be tested using the Costa Rica Aura Validation Experiment (CRAVE) data. Figure 8 shows the CRAVE CO_2 data used by *Park et al.* [2007] on four isentropic surfaces in the TTL. A daily average value for each level is calculated (red diamonds) and using the observed variability to weight each daily mean, a best fit trend line is calculated for surfaces from 360 to 390 K (red line). The slope of the time trend is inversely proportional to the transit time under the assumption that vertical advection plays the dominant role.

[28] Our analysis shows that the variability at 360 K is very large and there is no statistically significant trend (time-varying signal) as required to use CO_2 to estimate the vertical velocity. The fits to points for 370–390 K do give trends although the uncertainties are ~30% at each level. The trends at each level are less than half the trend in the Boering proxy. This also suggests that simple upward advection model cannot be used to estimate the transit time.

[29] Since there is no clear trend in CO_2 at 360 K, we cannot use that level to estimate the velocity. However, the similarity of the trends from 370 to 390 K suggests it may be possible to estimate transit time/vertical velocity between these levels. Using the daily mean values and uncertainties at 390 and 370 K for each flight, we calculate the daily mean vertical gradient for the 10 flight days to be -0.52 ± 0.19 ppm/20 K. Propagating the uncertainties in each isentropic mean (~0.14 ppm) gives a 37% uncertainty in the gradients. Using the $\Delta t = \Delta z \frac{\langle \partial CO_2 / \partial z \rangle}{\partial CO_2 / \partial t}$ (where the angle brackets indicate time mean) to estimate transit times, we find a transit time of 35 ± 17 days for the transit from 370 to 390 K. This result is significantly different from the *Park et al.* [2007] estimates of 26 ± 3 or 28 ± 10 days (using two different estimates of the vertical gradient) for transit from 360 to 390 K. The reasons for the large difference are (1) we omit the 360 K data because they show no time-varying signal, (2) we calculate the actual time-varying signal at 370 K rather than assuming the Boering proxy, resulting in a much smaller time trend, and (3) we propagate larger uncertainties from the gradient and time trend into the
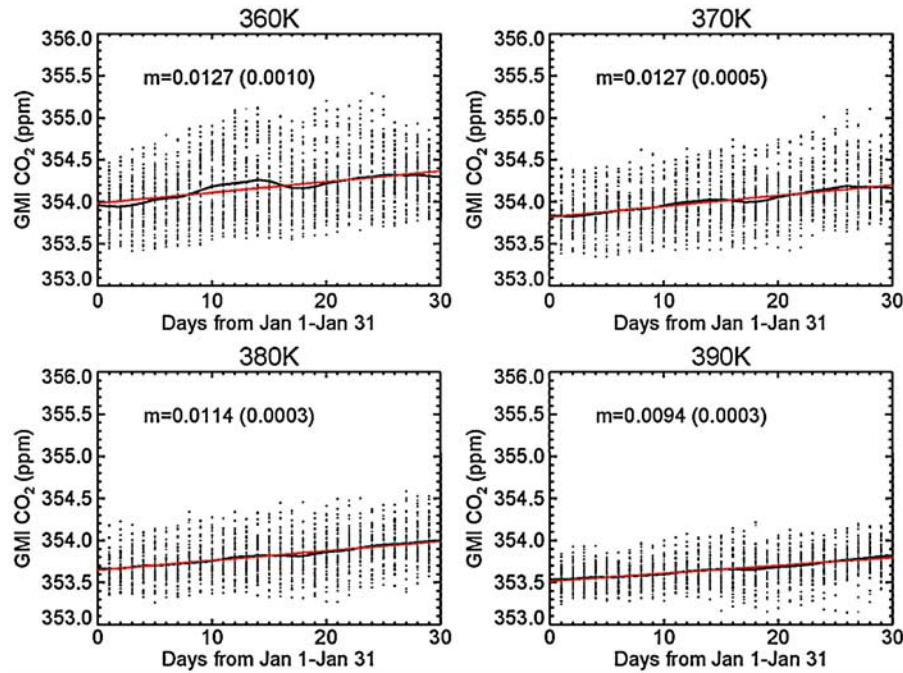
Figure 9. Changes in CO_2 at different isentropic surfaces in the GMI-CTM between $10°S$ and $10°N$ over a sequence of 30 days. Dots indicate values, and solid line is the mean.

calculation. Using the CRAVE altitude data, transport from 370 to 390 K covers a distance of 1.8 km (16.0–17.8 km). Assuming that all the change is due to pure upward advection the estimated vertical velocity is 0.06 ± 0.03 cm/s. This value is closer to the estimates from the water vapor tape recorder although still somewhat too high.

[30] The CO_2 measurements were taken during the NH winter and the BDC vertical velocity is stronger during that season. Thus, we expect that the CO_2 estimate at the tropopause ($\sim$370 K) will be higher than the water vapor tape recorder multiyear average of the vertical velocity. From the models, the annual amplitude of the BDC is about $0.01–0.02$ cm/s at 18 km [*Schoeberl et al.*, 2008] which when added to the mean values of 0.04 cm/s (Figure 7) comes closer to the CO_2 estimate of 0.06 ± 0.03 cm/s estimated here and is within our uncertainty.

4.3. CO_2 and Vertical Velocities in the Global Modeling Initiative–Chemical Transport Model

[31] In this section we go one step further and apply the technique used by *Park et al.* [2007] to CO_2 simulated by the Global Modeling Initiative–Chemical Transport Model (GMI-CTM). The advantage of this approach is that we can actually evaluate all the processes leading to changes in CO_2 in the lower tropical stratosphere. This simulation uses the GEOS-4 GCM met fields at $2°$ latitude by $2.5°$ longitude resolution with vertical spacing of $0.9–1.0$ km in the UT/LS. The excellent fidelity of UT/LS transport in this model was determined using multiple transport diagnostics given by *Strahan et al.* [2007] and further demonstrated by realistic transport of biomass burning pollutants through the TTL given by *Duncan et al.* [2007]. CO_2 boundary conditions in the CTM were derived from NOAA CMDL surface measurements from 1977 to 1993 [*Conway et al.*, 1994]. To apply the clock tracer method, we use the model TTL time

series to determine the actual time-varying stratospheric input rather than the Boering proxy. Model time series for January on four isentropic levels in the tropics ($10°S–10°N$) are shown in Figure 9. Note that the model variability is very similar to that observed during CRAVE. Observed and modeled variability at 360 K is greater than 1 ppm daily, which suggests that the sparse sampling of aircraft data would make a $\sim$0.4 ppm/month trend difficult to detect.

[32] We determine the mean model CO_2 vertical gradient by differencing mixing ratios at 370 and 390 K for each tropical profile for each day in January. The mean gradient, 0.36 ± 0.19 ppm/20 K, is used to calculate a transit time based on the model CO_2 growth rate of 0.015 ppm/d at 370 K, which is the same as the observed growth rate shown in Figure 8. The resulting transit time is 24 ± 13 days, however, since 370–390 K in the GMI-CTM spans 1.4 km rather than the 1.8 km measured during CRAVE, the resulting mean vertical velocity is 0.068 ± 0.037 cm/s. While the model's temperature structure results in different layer thicknesses between 370 and 390 K, the net upward transport of the time-varying CO_2 signal in the model TTL is very similar to observed during CRAVE and applying the tracer method gives the same estimate of vertical velocity for both data and model. The GEOS-4 GCM vertical velocities averaged over $10°S–10°N$ in January range from 0.05 to 0.014 cm/s from 370 to 390 K. The average over this height range, 0.03 cm/s, is half the vertical velocity derived using the CO_2 observations and the CTM simulation.

[33] Why does CO_2 as a tracer of upward advection produce an apparent vertical velocity value almost twice as large as the actual vertical velocity? In the calculations above, the tracer tendency equation, which defines $\partial CO_2/\partial t$, is assumed to have only one significant term: $\bar{w}\partial CO_2/\partial z$, where $\bar{w}$ is the mean vertical velocity. However, the tendency equation also includes vertical and horizontal eddy

Table 2. CO_2 Tendency Budget in the TTL for January[a]

	$\partial CO_2/\partial t$ ($\times 10^6$ ppm/s)	Vertical Velocity (w) (cm/s)	Vertical Advection ($\times 10^6$ ppm/s)	Horizontal Eddy ($\times 10^6$ ppm/s)	Vertical Eddy ($\times 10^6$ ppm/s)	Sum of Terms ($\times 10^6$ ppm/s)
Lower TTL						
360 K	0.144	0.092	0.078	−0.139	0.202	0.140
370 K	0.130	0.043	0.069	−0.075	0.119	0.113
Upper TTL						
380 K	0.103	0.051	0.107	−0.031	0.031	0.107
390 K	0.078	0.040	0.100	−0.055	0.023	0.069

[a]The tropical tropopause layer (TTL) is separated into a lower and upper region in this calculation because the latitude range of ascent shifts with height. Ascent occurs from roughly 20°S to 10°N at 360–370 K, while at 380–390 K, ascent shifts southward from approximately 24°S to the equator.

transport processes. The terms of the CO_2 tendency equation in the TTL calculated from the GMI-GCM simulation are given in Table 2. The vertical advection term, $\bar{w}\partial CO_2/\partial z$, accounts for just over half of the total tendency from 360 to 370 K. Calculation of the horizontal eddy transport term shows that its contribution is negative, meaning that lower CO_2 is mixed into the tropics from extratropical regions; this term is largest in the lower TTL (see Table 2). The vertical eddy transport is positive; and accounts for transport of CO_2 upward across the tropical vertical gradient. The vertical eddy transport term is similar in size but opposite in sign to the horizontal eddy term; thus, the two eddy transport terms mostly cancel. Nonetheless, their net effect is to add to the CO_2 tendency term almost as much as the mean vertical advection term in the lower TTL, in effect doubling the number.

[34] In the upper TTL (380–390 K), the vertical advection term dominates the tendency. The eddy terms are smaller but not negligible. Thus, assuming that the tendency is due only to a mean transport vertical velocity will lead to an overestimate of that vertical velocity because the tendency includes terms for eddy transport as well as advective transport. In the case of the water vapor tape recorder, the mean vertical and horizontal gradients of water vapor are small in the upper TTL so the eddy terms do not contribute to the tendency. Thus, the water vapor tendency can be used to diagnose the mean vertical velocity.

[35] The excellent agreement between the modeled and observed CO_2 trends and vertical gradients lends strong credibility to model transport processes in the TTL. The difference between the CO_2 tendency and vertical advection terms, particularly below 380 K, shows that the other terms in the tendency equation are not negligible, and thus, the presence of vertical and meridional gradients in CO_2 makes it difficult to use CO_2 as a diagnostic of the vertical velocity in the TTL.

5. Summary

[36] We use the water vapor tape recorder signal from HALOE and MLS data to diagnose the magnitude of the time mean, zonal mean tropical upwelling circulation. The method is to simply compute the lag correlation between levels to identify time for the propagation of the signal between levels. We test the method using the CGCM output which contains a tape recorder signal. In general the method

tends to slightly overestimate the vertical velocity but overall provides a reasonable estimate. With HALOE and MLS data, we find the vertical velocity to be <0.04 cm/s below 28 km. We also observe a minimum in vertical velocity near 19 km. These results are in good agreement with previous estimates from water vapor [*Mote et al.*, 1996, 1998; *Niwano et al.*, 2003], the GEOS-4 CCM and other model analyses of the transport vertical velocity [*Randel et al.*, 2008]. Our results also agree with radiative transfer calculations by *Rosenlof* [1995] and more recently by *Fu et al.* [2007]. Our results do not agree with estimates of the vertical upwelling given by *Park et al.* [2007] as diagnosed from CO_2 measurements made from high-altitude aircraft. *Park et al.* [2007] estimate the upwelling rate is 0.15 cm/s.

[37] To explain the discrepancy between our results and those of *Park et al.* [2007] we also diagnose the aircraft data. Our analysis yields a mean vertical velocity of about 0.06 ± 0.03 cm/s, considerably smaller than that reported by *Park et al.* [2007] Still, this number is higher than the 0.04 cm/s for winter (although within the uncertainty) derived from the observed and modeled water vapor tape recorder. Using the GMI CO_2 simulation we note that the assumption that all the CO_2 transport is simply due to the mean upward advection term cannot be justified. Vertical eddy transport of CO_2 accounts for nearly half the tendency and cannot assumed to be zero. This result implies that the corrected vertical velocity diagnosed from CO_2 should be about half of 0.06 ± 0.03 cm/s or ~ 0.03 cm/s, in good agreement with the models and the upwelling velocity derived from the water vapor tape recorder.

References

Andrews, A. E., et al. (1999), Empirical age spectra for the lower tropical stratosphere from in situ observations of CO_2: Implications for stratospheric transport, *J. Geophys. Res.*, *104*, 26,581–26,595, doi:10.1029/1999JD900150.

Andrews, D. G., J. R. Holton, and C. B. Leovy (1987), *Middle Atmosphere Dynamics*, 489 pp., Academic, San Diego, Calif.

Baldwin, M. P., et al. (2001), The quasi-biennial oscillation, *Rev. Geophys.*, *39*, 179–229.

Bloom, S. C., et al. (2005), The Goddard Earth Observation System Data Assimilation System, GEOS DAS version 4.0.3: Documentation and validation, *NASA TM-2005-104606*, vol. 26.

Boering, K. A., S. C. Wofsy, B. C. Daube, H. R. Schneider, M. Loewenstein, and J. R. Podolske (1996), Stratospheric mean ages and transport rates

from observations of carbon dioxide and nitrous oxide, *Science*, *274*(5291), 1340–1343, doi:10.1126/science.274.5291.1340.

Conway, T. J., P. P. Tans, L. S. Waterman, K. W. Thoning, D. R. Kitzis, K. A. Masarie, and N. Zhang (1994), Evidence for interannual variability of the carbon cycle from the NOAA Climate Monitoring and Diagnostics Laboratory Global Air Sampling Network, *J. Geophys. Res.*, *99*, 22,831–22,855, doi:10.1029/94JD01951.

Corti, T., B. P. Luo, Q. Fu, H. Vomel, and T. Peter (2006), The impact of cirrus clouds on the tropical troposphere-to-stratosphere transport, *Atmos. Chem. Phys.*, *6*, 2539–2547.

Douglass, A. R., M. R. Schoeberl, R. B. Rood, and S. Pawson (2003), Evaluation of transport in the lower tropical stratosphere in a global chemistry and transport model, *J. Geophys. Res.*, *108*(D9), 4259, doi:10.1029/2002JD002696.

Duncan, B. N., S. E. Strahan, Y. Yooshida, S. D. Steenrod, and N. Livesey (2007), Model of the cross-tropopause transport of biomass burning pollution, *Atmos. Chem. Phys.*, *7*, 3713–3736.

Dunkerton, T. J. (1991), Nonlinear propagation of zonal winds in an atmosphere with Newtonian cooling and equatorial wavedriving, *J. Atmos. Sci.*, *48*, 236–263, doi:10.1175/1520-0469(1991)048<0236:NPOZWI>2.0.CO;2.

Eluszkiewicz, J., et al. (1996), Residual circulation in the stratosphere and lower mesosphere derived from Microwave Limb Sounder data, *J. Atmos. Sci.*, *53*, 217–240, doi:10.1175/1520-0469(1996)053<0217:RCITSA>2.0.CO;2.

Eyring, V., et al. (2006), Assessment of temperature, trace species, and ozone in chemistry-climate model simulations of the recent past, *J. Geophys. Res.*, *111*, D22308, doi:10.1029/2006JD007327.

Folkins, I., P. Bernath, C. Boone, G. Lesins, N. Livesey, A. M. Thompson, K. Walker, and J. C. Witte (2006), Seasonal cycles of O_3, CO, and convective outflow at the tropical tropopause, *Geophys. Res. Lett.*, *33*, L16802, doi:10.1029/2006GL026602.

Fu, Q., Y. Hu, and Q. Yang (2007), Identifying the top of the tropical tropopause layer from vertical mass flux analysis and CALIPSO lidar cloud observations, *Geophys. Res. Lett.*, *34*, L14813, doi:10.1029/2007GL030099.

Haynes, P. H., et al. (1991), On the downward control of extratropical diabatic circulations by eddy-induced mean zonal forces, *J. Atmos. Sci.*, *48*, 651–679.

Kerr-Munslow, A. M., and W. A. Norton (2006), Tropical wave driving of the annual cycle in tropical tropopause temperatures. Part I. ECMWF analyses, *J. Atmos. Sci.*, *63*, 1410–1419, doi:10.1175/JAS3697.1.

Lambert, A., et al. (2007), Validation of the Aura Microwave Limb Sounder middle atmosphere water vapor and nitrous oxide measurements, *J. Geophys. Res.*, *112*, D24S36, doi:10.1029/2007JD008724.

Liu, C., and E. J. Zipser (2005), Global distribution of convection penetrating the tropical tropopause, *J. Geophys. Res.*, *110*, D23104, doi:10.1029/2005JD006063.

Mote, P. W., K. H. Rosenlof, M. E. McIntyre, E. S. Carr, J. C. Gille, J. R. Holton, J. S. Kinnersley, H. C. Pumphrey, J. M. Russell, and J. W. Waters (1996), An atmospheric tape recorder: The imprint of tropical tropopause temperatures on stratospheric water vapor, *J. Geophys. Res.*, *101*, 3989–4006, doi:10.1029/95JD03422.

Mote, P. W., T. J. Dunkerton, M. E. McIntyre, E. A. Ray, P. H. Haynes, and J. M. Russell III (1998), Vertical velocity, vertical diffusion and dilution by midlatitude air in the tropical lower stratosphere, *J. Geophys. Res.*, *103*, 8651–8666, doi:10.1029/98JD00203.

Niwano, M., K. Yamazaki, and M. Shiotani (2003), Seasonal and QBO variations of the ascent rate in the tropical lower stratosphere as inferred from UARS HALOE trace gas data, *J. Geophys. Res.*, *108*(D24), 4794, doi:10.1029/2003JD003871.

Norton, W. A. (2006), Tropical wave driving of the annual cycle in tropical tropopause temperatures. Part II: Model results, *J. Atmos. Sci.*, *63*, 1420–1431, doi:10.1175/JAS3698.1.

Oman, L., D. W. Waugh, S. Pawson, R. S. Stolarski, and J. E. Nielsen (2008), Understanding the changes of stratospheric water vapor in coupled chemistry-climate model simulations, *J. Atmos. Sci.*, *65*, 3278–3291.

Park, S., et al. (2007), The CO_2 tracer clock for the tropical tropopause layer, *Atmos. Chem. Phys.*, *7*, 3989–4000.

Pawson, S. R., S. Stolarski, A. R. Douglass, P. A. Newman, J. E. Nielsen, S. M. Frith, and M. L. Gupta (2008), Goddard Earth Observing System chemistry-climate model simulations of stratospheric ozone-temperature coupling between 1950 and 2005, *J. Geophys. Res.*, *113*, D12103, doi:10.1029/2007JD009511.

Pumphrey, H. C., C. Boone, K. A. Walker, P. Bernath, and N. J. Livesey (2008), The tropical tape recorder observed in HCN, *Geophys. Res. Lett.*, *35*, L05801, doi:10.1029/2007GL032137.

Randel, W. J., F. Wu, H. Vömel, G. E. Nedoluha, and P. Forster (2006), Decreases in stratospheric water vapor after 2001: Links to changes in the tropical tropopause and the Brewer-Dobson circulation, *J. Geophys. Res.*, *111*, D12312, doi:10.1029/2005JD006744.

Randel, W., M. Park, F. Wu, and N. Livesey (2007), A large annual cycle in ozone above the tropical tropopause linked to the Brewer-Dobson circulation, *J. Atmos. Sci.*, *64*, 4479–4488, doi:10.1175/2007JAS2409.1.

Randel, W., R. Garcia, and F. Wu (2008), Dynamical balances and tropical stratospheric upwelling, *J. Atmos. Sci.*, doi:10.1175/2008JAS2756.1, in press.

Rayner, N. A., D. E. Parker, E. B. Horton, C. K. Folland, L. V. Alexander, D. P. Rowell, E. C. Kent, and A. Kaplan (2003), Global analyses of sea surface temperature, sea ice, and night marine air temperature since the late nineteenth century, *J. Geophys. Res.*, *108*(D14), 4407, doi:10.1029/2002JD002670.

Read, W., et al. (2007), Aura Microwave Limb Sounder upper tropospheric and lower stratospheric H_2O and relative humidity with respect to ice validation, *J. Geophys. Res.*, *112*, D24S35, doi:10.1029/2007JD008752.

Rosenlof, K. (1995), Seasonal cycle of the residual mean meridional circulation in the stratosphere, *J. Geophys. Res.*, *100*, 5173–5191, doi:10.1029/94JD03122.

Rosenlof, K. H., A. F. Tuck, K. K. Kelly, J. M. Russell, and M. P. McCormick (1997), Hemispheric asymmetries in water vapor and inferences about transport in the lower stratosphere, *J. Geophys. Res.*, *102*, 13,213–13,234.

Russell, J. M., III, L. L. Gordley, J. H. Park, S. R. Drayson, W. D. Hesketh, R. J. Cicerone, A. F. Tuck, J. E. Frederick, J. E. Harries, and P. J. Crutzen (1993), The Halogen Occultation Experiment, *J. Geophys. Res.*, *98*, 10,777–10,797, doi:10.1029/93JD00799.

Schoeberl, M., A. E. Roche, J. M. Russell III, D. Ortland, P. B. Hays, and J. W. Waters (1997), An estimation of the dynamical isolation of the tropical lower stratosphere using UARS wind and trace gas observations of the quasi-biennial oscillation, *Geophys. Res. Lett.*, *24*, 53–56.

Schoeberl, M. R., B. N. Duncan, A. R. Douglass, J. Waters, N. Livesey, W. Read, and M. Filipiak (2006), The carbon monoxide tape recorder, *Geophys. Res. Lett.*, *33*, L12811, doi:10.1029/2006GL026178.

Schoeberl, M. R., et al. (2008), QBO and annual cycle variations in tropical lower stratosphere trace gases from HALOE and Aura MLS observations, *J. Geophys. Res.*, *113*, D05301, doi:10.1029/2007JD008678.

Shepherd, T. G. (2007), Transport in the middle atmosphere, *J. Meteorol. Soc. Jpn.*, *85B*, 165–191.

Strahan, S., B. N. Duncan, and P. Hoor (2007), Observationally derived transport diagnostics for the lowermost stratosphere and their application to the GMI chemistry and transport model, *Atmos. Chem. Phys.*, *7*, 2435–2445.

Waters, J., et al. (2006), The Earth Observing System Microwave Limb Sounder (EOS MLS) on the Aura satellite, *IEEE Trans. Geosci. Remote Sens.*, *44*, 1075–1092, doi:10.1109/TGRS.2006.873771.

Waugh, D., and T. Hall (2002), Age of stratospheric air: Theory, observations and models, *Rev. Geophys.*, *40*(4), 1010, doi:10.1029/2000RG000101.

―――――――――

A. R. Douglass, S. Pawson, M. R. Schoeberl, and R. S. Stolarski, NASA Goddard Space Flight Center, Mail Stop 613.3, Code 910, Greenbelt, MD 20771, USA. (mark.r.schoeberl@nasa.gov)

W. Read, Jet Propulsion Laboratory, California Institute of Technology, 4800 Oak Grove Drive, Pasadena, CA 91109, USA.

S. E. Strahan, Goddard Earth Science and Technology Center, University of Maryland, Baltimore County, 5523 Research Park Drive, Suite 320, Baltimore, MD 21228, USA.